Supporting Information

Electrochemical Regeneration of Amine-Based CO_2 Capture System: A Study on CO_2 Desorption Efficiency

Barbara Bohlen[a], Luis F. Leon-Fernandez[a], Nick Daems[a], Tom Breugelmans[a]

[a] Research Group Applied Electrochemistry and Catalysis (ELCAT), University of Antwerp, Universiteitsplein 1, 2610 Wilrijk, Belgium.

* corresponding author: tom.breugelmans@uantwerpen.be

Figure S1: electrochemical cells used for the CV studies. Left: 1-comparment cell with Cu WE, Ag/AgCl RE and Pt-Ti mesh CE (used for pH variation and different WEs).Right: H-cell with resin anode side and glass cathode side (used for LSV and CVs at different temperatures), Cu WE, mini Ag/AgCl RE and 2x Pt-Ti mesh CE; designed with a jacket around the cell for temperature control. The resin half-cell was gas-tightly closed.

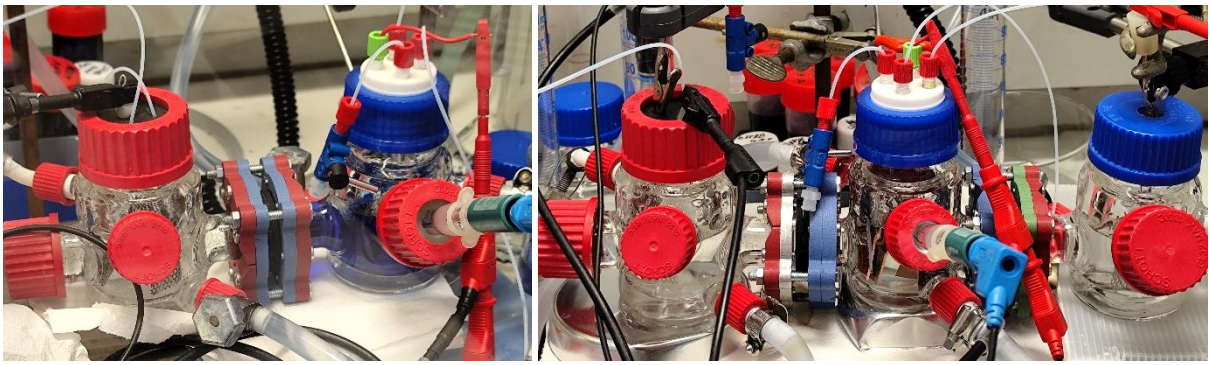

Figure S2: jacketed glass electrochemical cells used for the desorption experiments. Left: H-cell for the investigation of effect of current, surfactant and temperature. Right: three-compartment cell for the proof-of-concept experiments of pure e-acidification and combined e-dissolution + e-acidification. For both cells, the (middle) compartment containing the MEA solution to go through desorption was gas-tightly closed, with the gas outlet connected to the MFM and CO_2 sensor for quantification of the desorbed CO_2.

Absorption and chemical desorption experiments

Absorption experiments were carried out in a three-neck round-bottom flask containing 50 mL of the MEA solution (and the corresponding Cu loading) at 50 °C, in a gas-tight system. A condenser was attached to one neck to avoid evaporation of the electrolyte. CO_2 was purged at a constant flow rate of 50 SmL min^{-1}, controlled by a mass flow controller (MFC) and the gas flow out of the system was recorded by a mass flow meter (MFM), coupled to the CO_2 sensor, to obtain the concentration of CO_2 in the gas. This experiment was repeated three times for each Cu concentration in the MEA solution.

The chemical desorption experiments were carried out by placing 500 µL samples of each absorption experiment in a vial, at 50 °C, stirring at 400 rpm. 1 mL of 4 M H_2SO_4 was injected to the vial, to acidify the solution and force the full desorption of CO_2. The evolved gas was collected for 5 minutes with an in-house designed mechanical barometer, to ensure all the desorbed CO_2 was collected. This experiment was repeated 3 times for each sample and the average values and SD are presented in Table S1. Both setups are presented in the Figure S3.

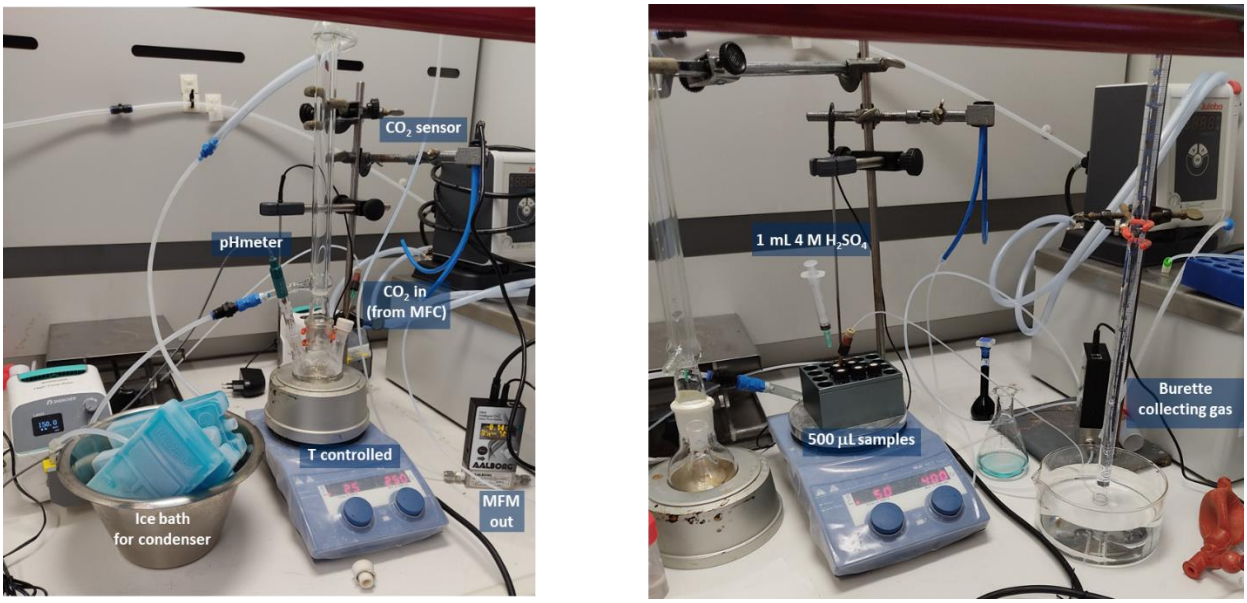

Figure S3: setups used for chemical absorption and desorption. Left: absorption setup, including 3-neck-roundbottom flask, condenser, heating plate to control the temperature, MFM, CO_2 sensor and pH meter. Right: desorption setup, including vial containing 500 µL samples, syringe with 4 M H_2SO_4,

heating plate to control the temperature and mechanical barometer to collect the evolved gas by the acid addition.

Table S1: mols of absorbed and desorbed for 5 M MEA solutions containing different concentrations of Cu, at 50°C. The chemical desorption was promoted by acidification of the samples with 4 M H_2SO_4.

Cu concentration / mol L^{-1}	**CO_2 absorbed / mol**	**CO_2 desorbed / mol**
0	0.139	0.091
0.5	0.112	0.081
1	0.080	0.054
1.5	0.053	0.040

An important parameter to characterize is the effect of the Cu concentration on the maximum CO_2 absorption, especially for integrated flow systems. As the EMAR system was idealized to work in recirculation, with the Cu-MEA anolyte being passed through the cathode after desorption, to electrodeposit the Cu and remove it from the solution, so the MEA can be reused in the absorption step. Therefore, it can be expected that some Cu will remain in solution as both processes will not be 100% complete at all times. The relation between Cu concentration and CO_2 absorption capacity can be established by promoting the CO_2 absorption in MEA solutions containing different concentrations of Cu.

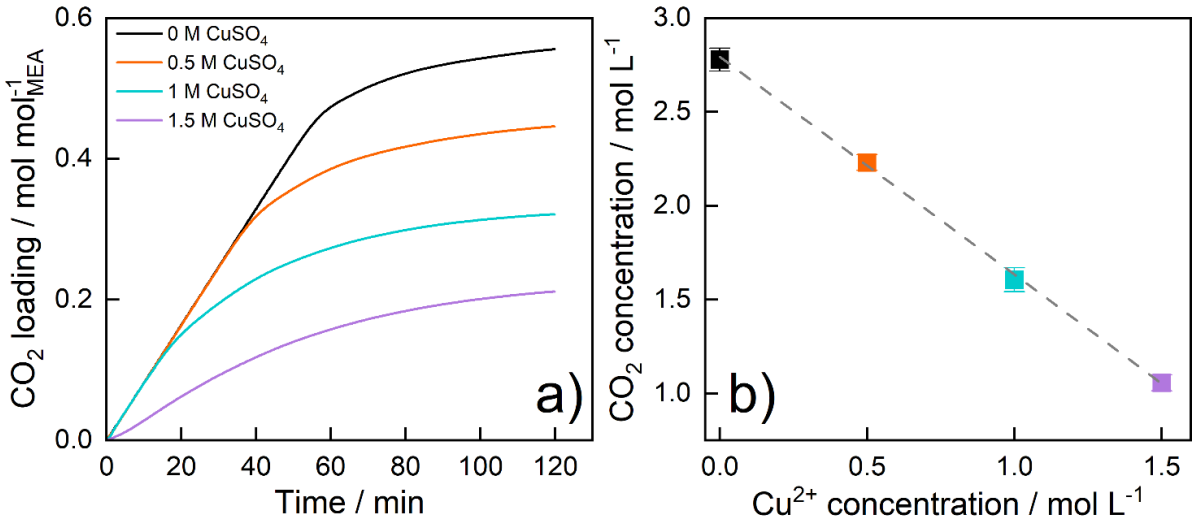

Figure S4: CO_2 saturation of 5 M MEA solutions with different concentrations of Cu in solution. Right: change in CO_2 loading with time, for solutions containing 0 M $CuSO_4 \cdot 5H_2O$ (black), 0.5 M $CuSO_4 \cdot 5H_2O$

(orange), 1 M $CuSO_4 \cdot 5H_2O$ (light green) and 1.5 M $CuSO_4 \cdot 5H_2O$ (lilac), CO_2 flow in: 50 SmL min^{-1}, at 50 °C; left plot: Cu^{2+} concentration vs. CO_2 concentration, both in mol L^{-1}, obtained for the absorption experiments at 50 °C, 50 mL solution.

Table S2: CO_2 concentration (in mol_{CO_2} mol_{MEA}^{-1} and mol_{CO_2} L^{-1}) at 50 °C, for solutions containing different $CuSO_4 \cdot 5H_2O$ concentrations

Cu concentration / mol L^{-1}	**CO_2 concentration / mol_{CO2} mol^{-1}_{MEA}**	**CO_2 concentration / mol_{CO2} L^{-1}**
0	0.572	2.86
0.5	0.446	2.23
1	0.321	1.61
1.5	0.211	1.06

From Figure S4 and Table S2, it can be observed that the maximal achieved loading of CO_2 decreases with increasing concentration of Cu, as expected, with 0.572 mol_{CO_2} mol_{MEA}^{-1} being the highest loading achieved at 50 °C for the pure MEA solution. With increasing amount of Cu in solution, more of the MEA is complexed with the metal ion and thus not available to capture CO_2. Not only does the higher concentration lead to lower CO_2 absorption, but also the relation between CO_2 and Cu concentrations appears to be linearly negative. From 0.5 to 1.5 M $CuSO_4$, the maximum CO_2 concentration went from 2.23 to 1.06 mol L^{-1}. Additionally, the absorption of CO_2 appears to start out fast but slows down with time until a plateau is reached. This is due to the fact that there are less free amines available, as a result, the probability for a MEA and CO_2 molecule to effectively collide and thus generate carbamate lowers until eventually the CO_2 absorption plateaus.

The absorption of CO_2 was also carried out for lower concentration of MEA (1 M) in the presence of Cu, see below Figure S5. For the 5 M MEA solution, the total concentration of captured CO_2 is higher than for the 1 M solution, as expected because there is more MEA to react with. On the contrary, at lower MEA concentration, the loading of mol_{CO_2} mol_{MEA}^{-1} is higher, because more CO_2 is captured as bicarbonate (in comparison to the 5 M MEA solution), via the CO_2 equilibria (presented in the reactions R_3 – R_6 in the manuscript), as there are more water molecules available, thus, it leads to a higher ratio

between CO_2 and MEA. It was also observed that the CO_2 saturation led to Cu precipitation more easily in the 1 M MEA solution as a light blue solid ($Cu(OH)_2$) was observed here, while no precipitate was observed for the highly concentrated amine. In both cases, the CO_2 capture leads to a similar shift in pH to lower values, from pH 10.7 to ca. 8.1 (for 5 M MEA) and from 10.4 to 7.7 for the 1 M MEA solution. However, for the 5 M solution, there is more MEA available to complex with the Cu, and the CO_2 saturation doesn't displace the Cu that is complexed, thus Cu remains soluble. Meanwhile, for the 1 M solution, the pH shift and the lower availability of MEA lead to the Cu in solution to precipitate.

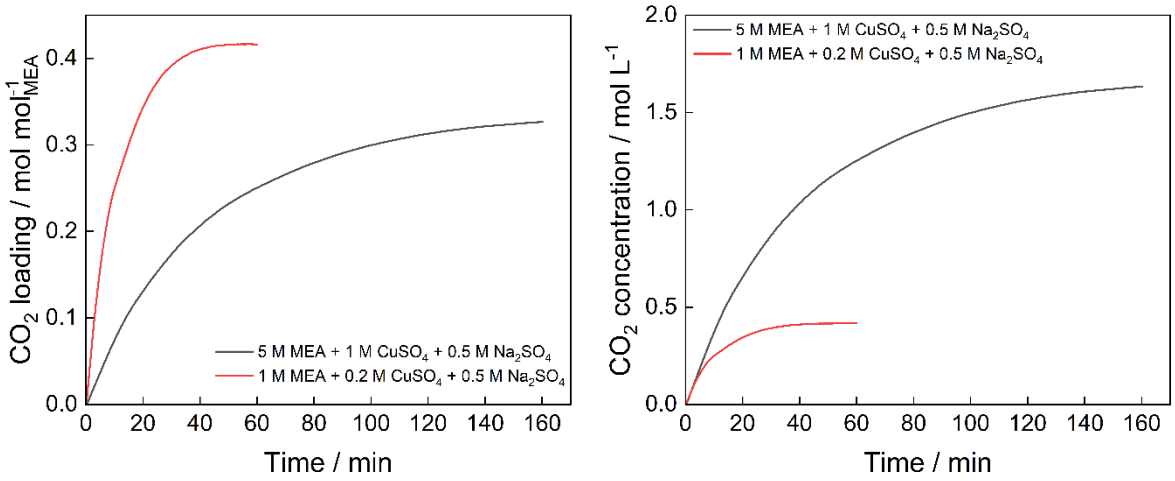

Figure S5: CO_2 saturation experiments carried out for two different concentrations of MEA: 5 M (black line) and 1 M (red line). Both solutions contained 0.5 M Na_2SO_4 as supporting electrolyte and a Cu loading of 0.2 mol_{Cu} mol_{MEA}^{-1}. Experiments carried out at 50 °C, with CO_2 inlet flow 50 SmL min^{-1}. On the left: loading of CO_2 in relation to the amount of MEA, i.e mol_{CO_2} mol_{MEA}^{-1}; on the right plot, concentration of CO_2 in mol L^{-1}. Electrolyte volume: 50 mL.

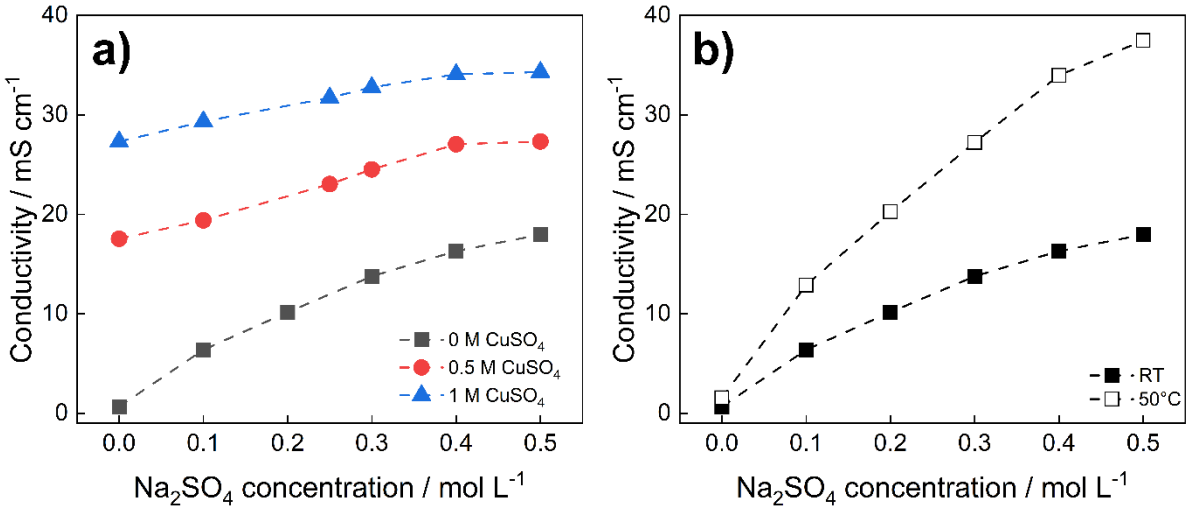

Figure S6: Conductivity of different solutions as a function of Na_2SO_4 concentration. a) conductivity values measured at 20 °C for 5 M MEA solutions containing 0 m $CuSO_4$ (black squares), 0.5 M $CuSO_4$ (red circles) and 1 M $CuSO_4$ (blue triangles) for Na_2SO_4 concentrations from 0 to 0.5 M; b) conductivity values measured for 5 M MEA solutions (with no $CuSO_4$) at RT (20 °C, black squares) and at 50 °C (white squares) with different concentrations of Na_2SO_4 (0 to 0.5 M).

Table S3: Conductivity of the 5 M MEA + 0.3 M Na_2SO_4 solutions, saturated with CO_2 or not, at 20, 25 and 50 °C.

Electrolyte	**Conductivity / mS cm^{-1}**		
	20 °C	**25 °C**	**50 °C**
5 M MEA + 0.3 M Na_2SO_4	12.4	13.8	27.2
5 M MEA + 0.3 M Na_2SO_4 + CO_2 sat.	40.8	44.9	65.3

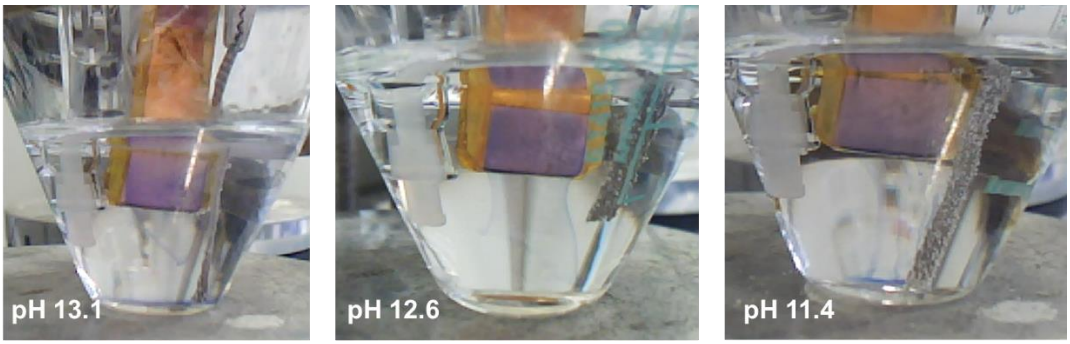

Figure S7: snapshot of recording of CV measurements at the three alkaline pHs: 13.1, 12.6 and 11.4. clear to see in all images is the dark blue Cu-MEA complex detaching from the electrode surface to the bottom of the cell.

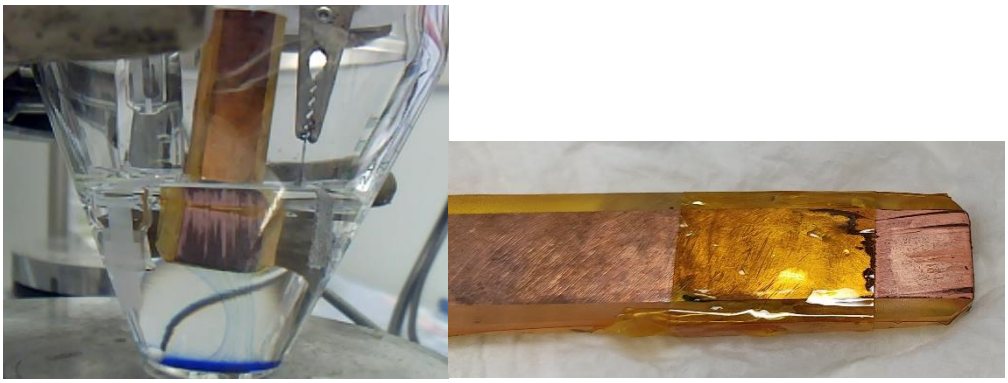

Figure S8: left: electrochemical cell for the CV measurement at pH 9.4, during the experiment, where the dark color, attributed to the copper oxides, is observed at the same time as the dark blue Cu-MEA complex detaching from the electrode surface. Right: image of the Cu WE after the CV, with some dark stains on its surface, also attributed to the formation of Cu oxides. It is important to highlight that the CV was stopped in the reduction direction.

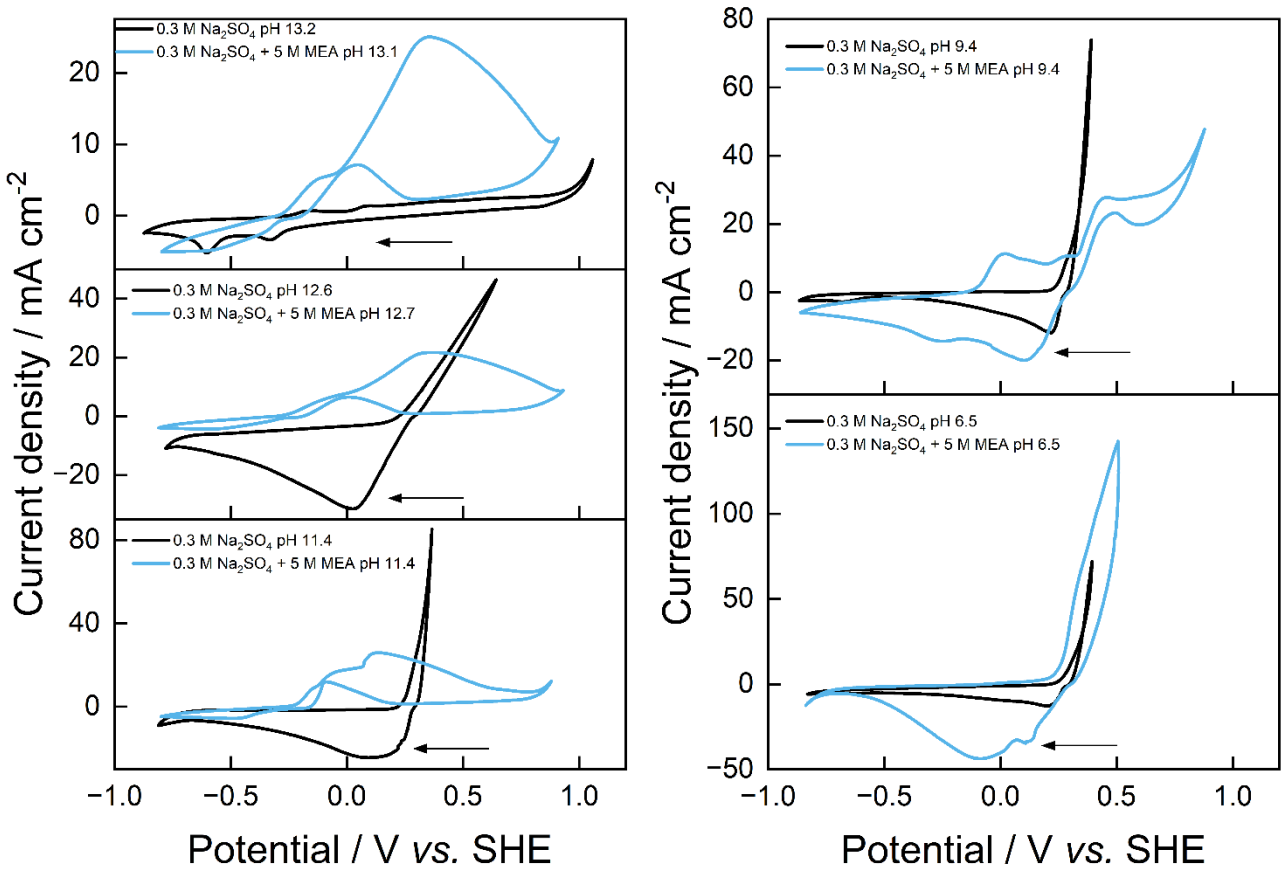

Figure S9: CVs obtained for a Cu WE at different pH values (indicated separately) in 0.3 M Na_2SO_4 solutions (black line) and 5 M MEA + 0.3 M Na_2SO_4 (blue line), scan rate: 20 mV s^{-1}, RE: Ag/AgCl, CE: Pt-Ti mesh. 100% iR drop compensation applied manually post-acquisition, electrolyte volume: 25 mL.

Figure S10: electrochemical cell during the CV measurement of 5 M MEA +0.3 M Na_2SO_4 at pH 6.5. The electrolyte has a light blue color due to the formation of $Cu(OH)_2$ and the electrode has a dark brown color on its surface, due to the formation of Cu oxides.

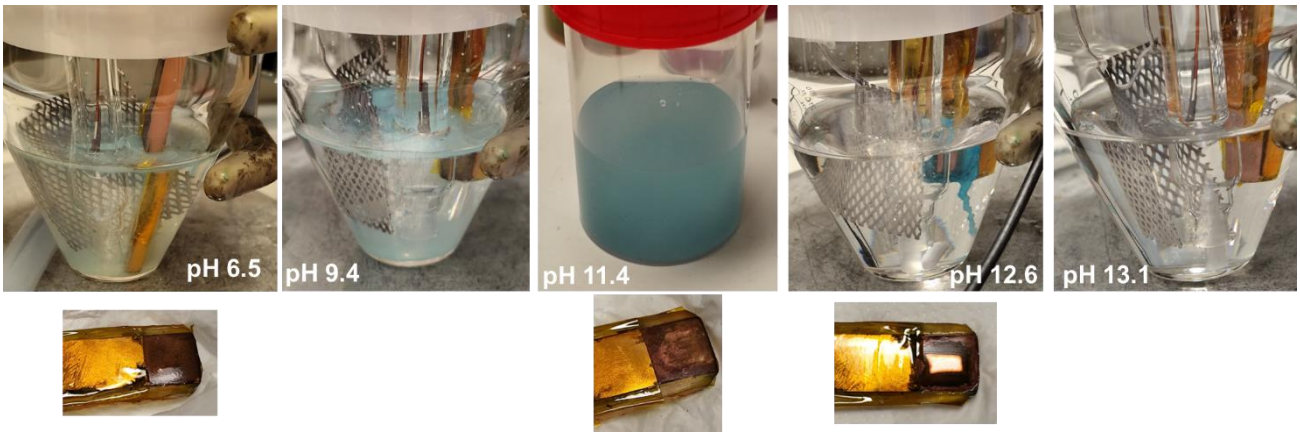

Figure S11: pictures of the electrolytes corresponding to each of the CVs obtained at pH values investigated for the 0.3 M Na_2SO_4 solutions. Inserted: pictures of the WEs surfaces after the CV.

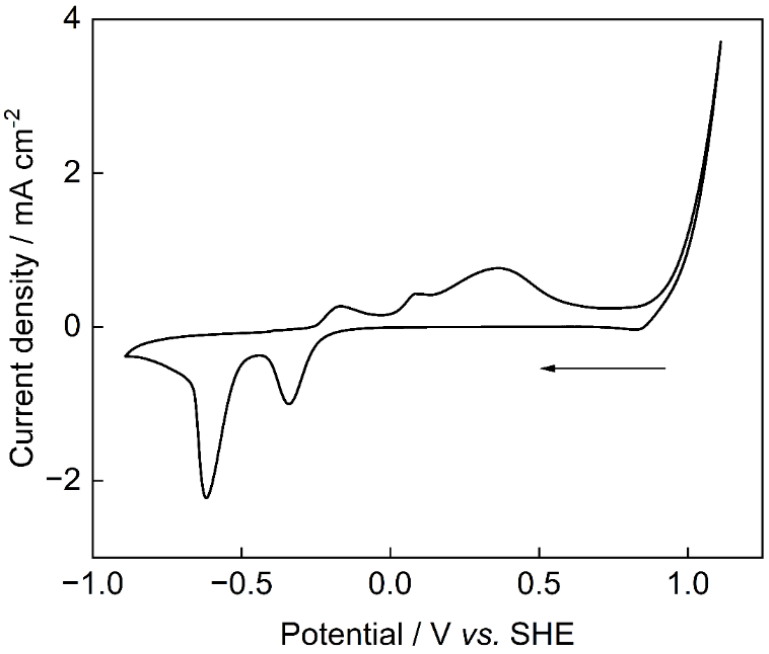

Figure S12: CV obtained with a Cu WE (1 cm^2) in 25 mL 0.1 M NaOH (pH 13), scan rate: 20 mV s^{-1}, RE: Ag/AgCl, CE: Pt-Ti mesh.

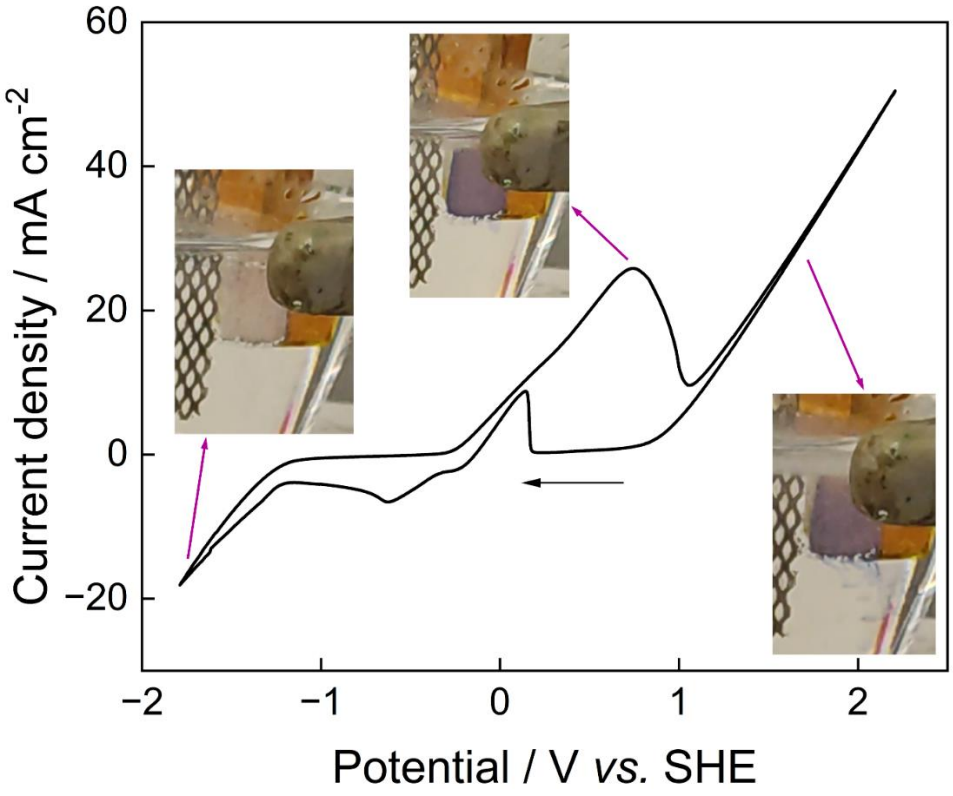

Figure S13: CV for 25 mL (CO_2-free) 5 M MEA + 0.3 M Na_2SO_4, scan rate: 50 mV s^{-1}, at RT, Cu WE (1 cm^2), Ag/AgCl RE and Pt-Ti mesh CE. Snapshots at selected potentials show bubble evolution only at E < –1.2 V vs. SHE (HER). During the anodic peak and subsequent current rise, no gas is observed; instead, a dark-blue plume forms at the WE, consistent with Cu oxidation and Cu–MEA complexation (no OER).

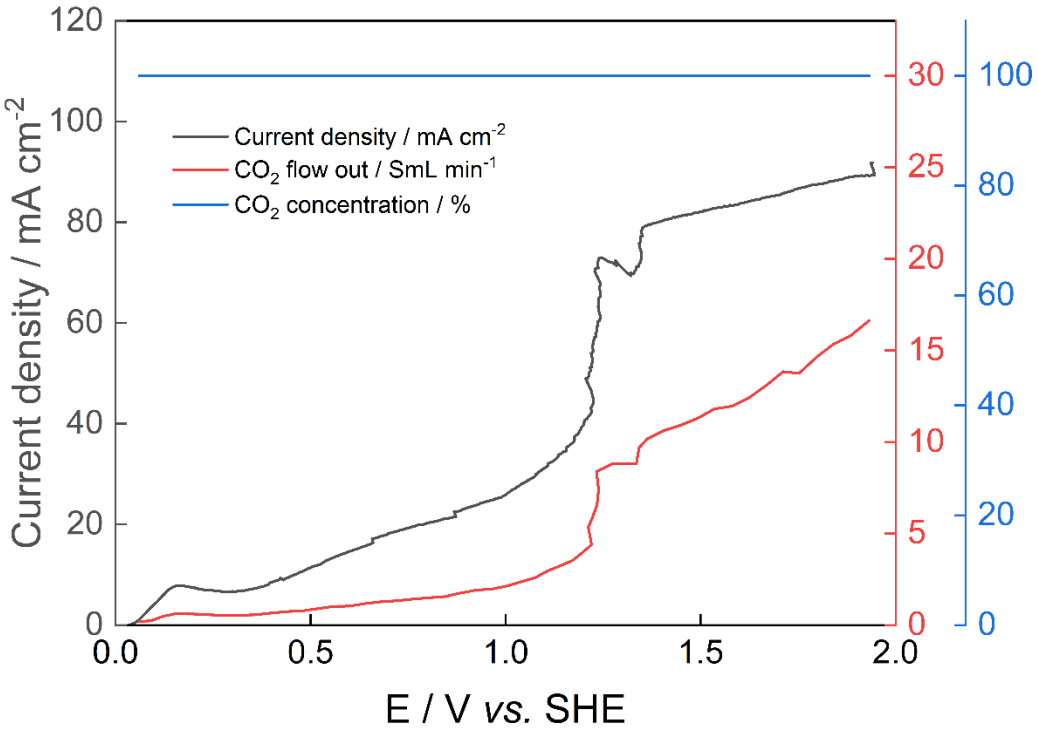

Figure S14: Linear sweep voltammetry of Cu electrodissolution of CO_2-saturated 5 M MEA + 0.3 M Na_2SO_4 with simultaneous monitoring of outlet gas flow rate and CO_2 concentration. Conditions: scan rate: 10 mV s^{-1}, pH 7.89, Cu plate WE (9.9 cm^2); Ag/AgCl RE; Pt-Ti mesh CE, 200 rpm stirring, anolyte volume: 60 mL; catholyte volume: 60 mL. Gray line: current density (mA cm^{-2}); red line: CO_2 flow out (SmL min^{-1}); blue line: CO_2 concentration (%).

The LSV was recorded in a gas tight H-cell, in which a Cu plate (9.9 cm^2) served as the working electrode in the anode compartment, separated from the cathode compartment (Pt–Ti mesh) by a Zirfon separator. During the sweep, the outlet gas stream from the anode compartment was continuously monitored for total flow and CO_2 concentration. The results indicate that the gas evolution increases proportionally with the current density, and the measured CO_2 fraction remains ~100% over the explored potential range. This indicates that the anodic gas evolution is dominated by CO_2 release, with no detectable contribution from OER under these conditions.

The current–potential trace exhibits pronounced fluctuations and irregular features, particularly at higher anodic potentials. This behavior is consistent with progressive modification of the Cu surface during electrodissolution/oxidation (*e.g.,* roughening, formation/removal of surface films and local inhomogeneities), combined with dynamic bubble coverage and imperfect convection near the

electrode, all of which can introduce transient mass-transport limitations and step-like features in the LSV.

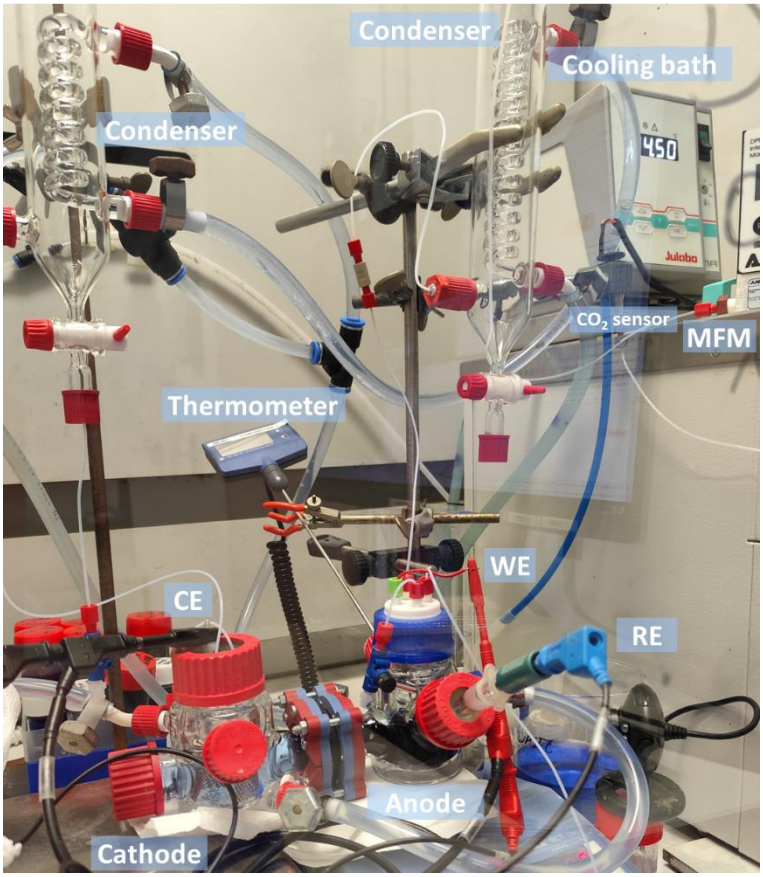

Figure S15: H-cell setup used for the study of the applied current on the CO_2 desorption efficiency. The following elements are indicated: cathode and anode side, WE, RE, CE, thermometer, condensers, MFM, CO_2 sensor and cooling bath.

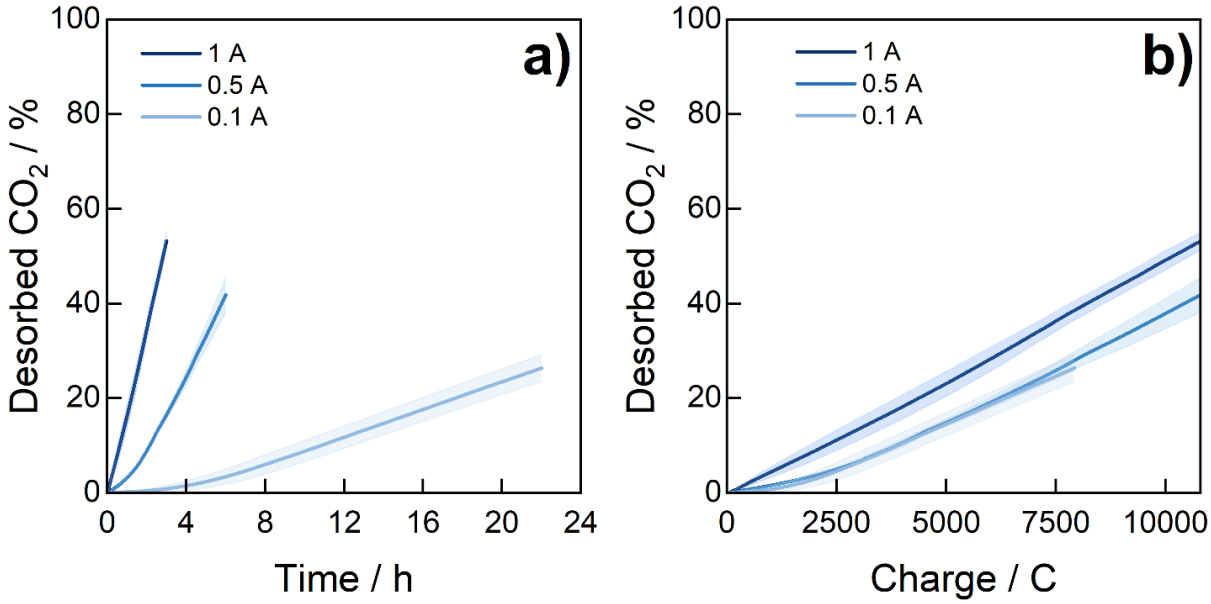

Figure S16: percentage of CO_2 desorbed from the 5 M MEA + 0.3 M Na_2SO_4 CO_2 saturated solution vs. a) time and b) charge, at different applied currents: 1, 0.5 and 0.1 A (gradient of blue from dark to light). Duplicate experiments represented by the average (dark line) and the maximum and minimum values (shaded region).

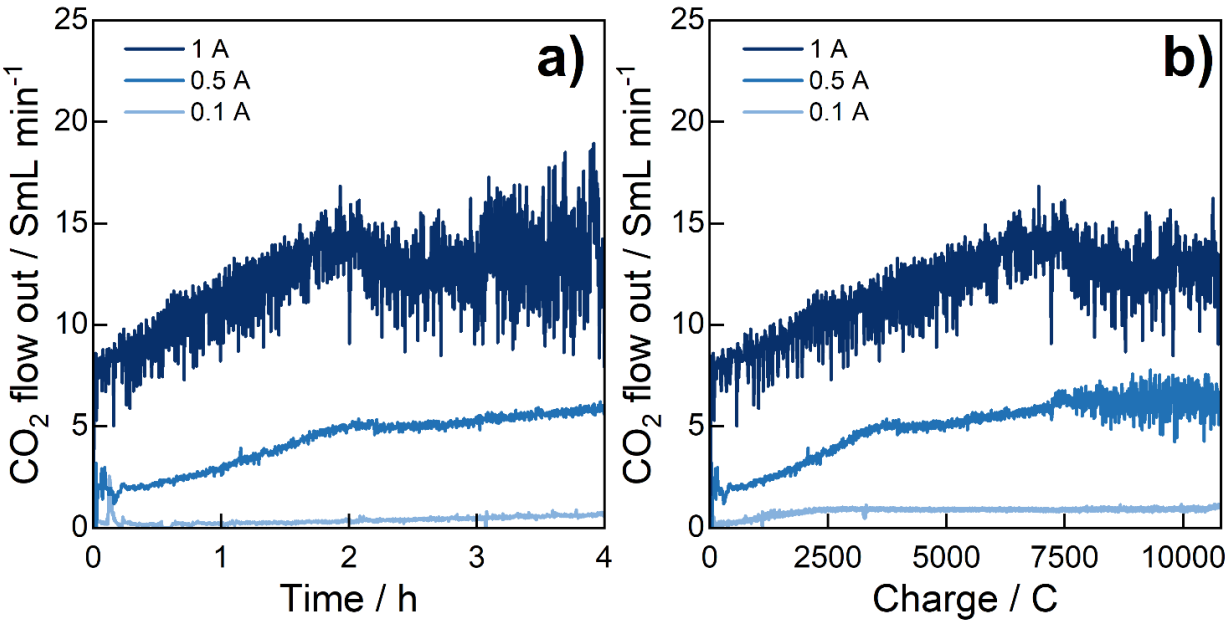

Figure S17: a) flow rate profile of the CO_2 desorption for each experiment at different currents vs. time (in h); b) flow rate profile of the CO_2 desorption for each experiment at different currents vs. charge. For both plots, the applied currents were 1, 0.5 and 0.1 A (gradient of blue, from dark to light, respectively).

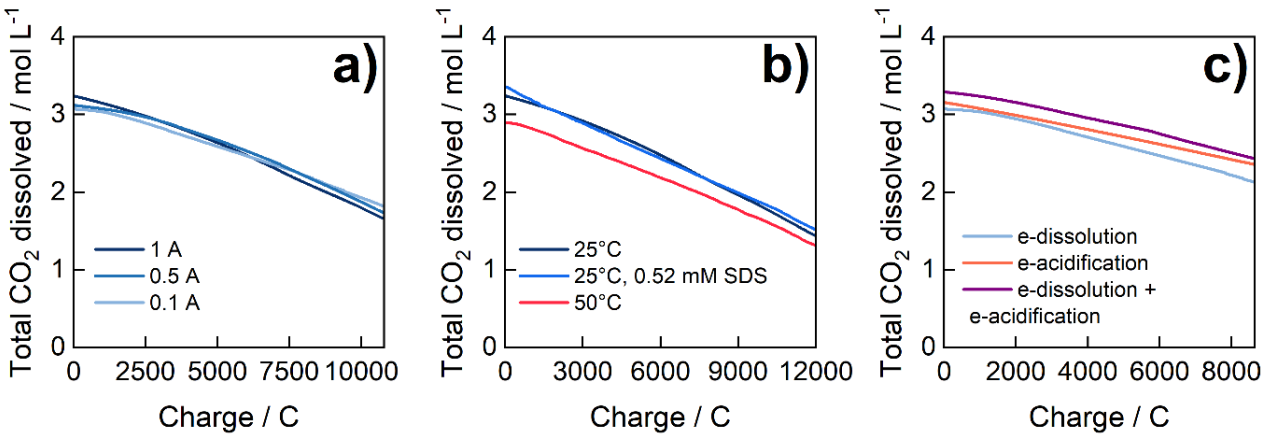

Figure S18: Evolution of dissolved CO_2 concentration (i.e., the sum of CO_2-derived aqueous species) as a function of passed charge during desorption experiments. a) different applied currents: 1, 0.5 and 0.1 A (gradient of blue from dark to light); b) at 1 A: without surfactant at 25 °C (dark blue), with SDS at 25 °C (light blue) and without SDS, at 50 °C (red); c) at 0.1 A, for e-dissolution (light blue), e-acidification (light red) and e-dissolution + e-acidification (purple). The comparisons are made at the maximal charge passed for each group of experiments. Experiments were carried out at controlled temperature, with Cu WE, Pt CE and Ag/AgCl RE, stirring: 500 rpm.

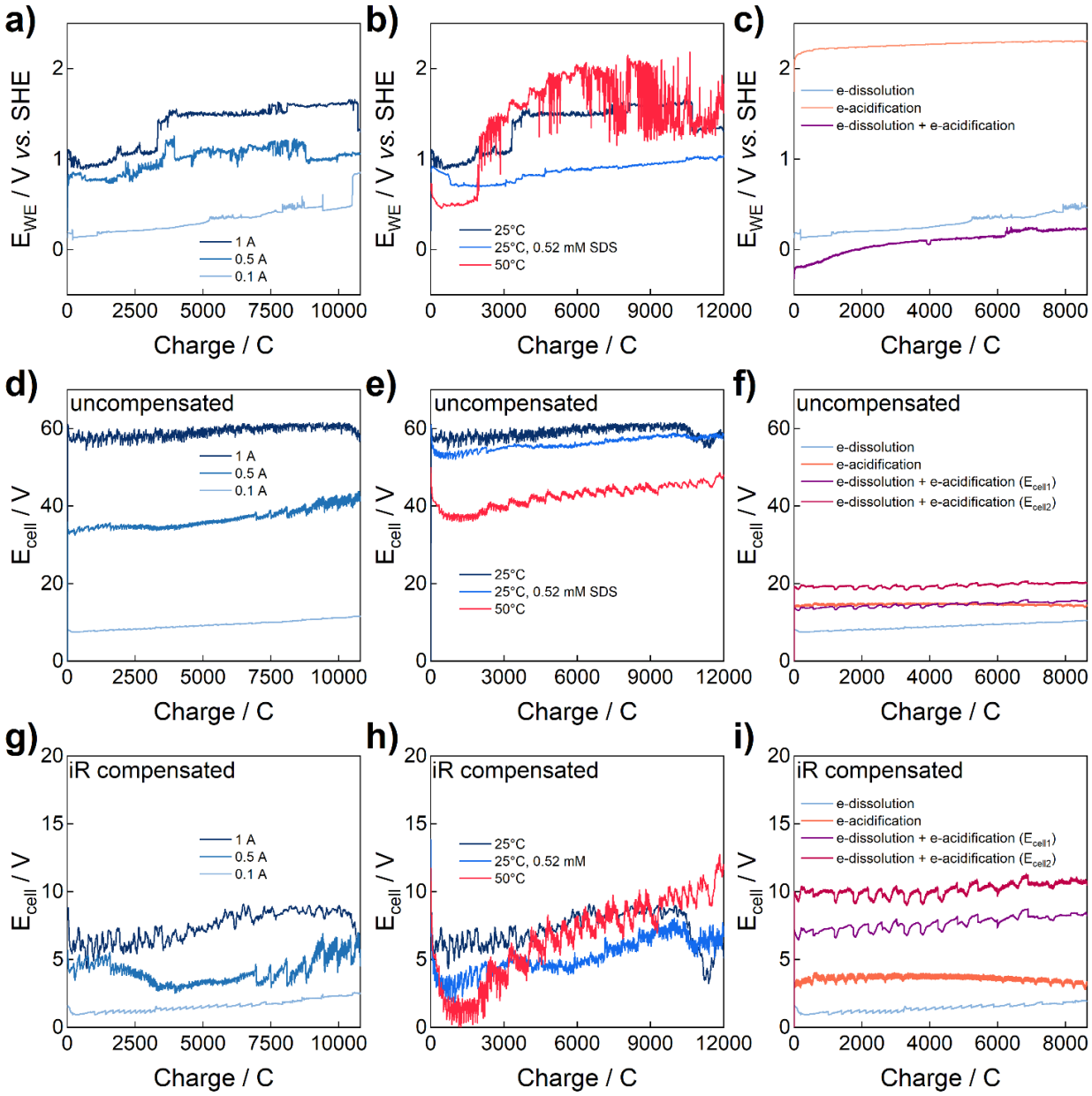

Figure S19: voltage profiles obtained for the desorption experiments with 5 M MEA + 0.3 M Na_2SO_4 CO_2 saturated solutions: a, b and c) working potential (vs. SHE) vs. charge; d, e and f) uncompensated cell potential vs. charge; g, h and i) iR compensated cell potential vs. charge. Results obtained at different parameters investigated: a, d and e) different applied currents: 1, 0.5 and 0.1 A (gradient of blue from dark to light); b, e and h) at 1 A: without surfactant at 25 °C (dark blue), with SDS at 25 °C (light blue) and without SDS, at 50 °C (red); c, f and i) at 0.1 A, for e-dissolution (light blue), e-acidification (light red) and e-dissolution + e-acidification (purple: WE_1-CE_1, dark red: WE_2-CE_2).

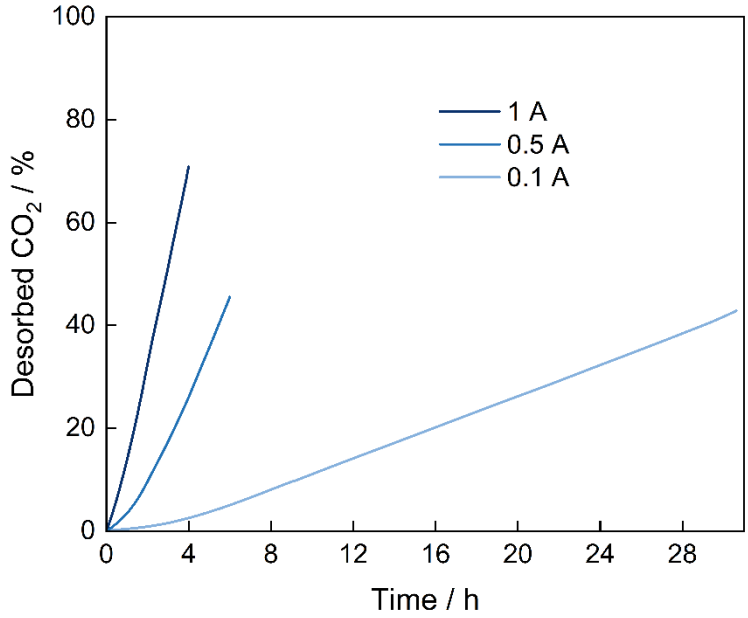

Figure S20: percentage of CO_2 desorbed from the 5 M MEA + 0.3 M Na_2SO_4 CO_2 saturated solution vs time, in h, at different applied currents: 1, 0.5 and 0.1 A (gradient of blue from dark to light).

Figure S21: pictures of the Cu WE after the desorption of CO_2 from 5 M MEA + 0.3 M Na_2SO_4 CO_2 saturated solutions, left at 1 A, middle at 0.5 A, right at 0.1 A.

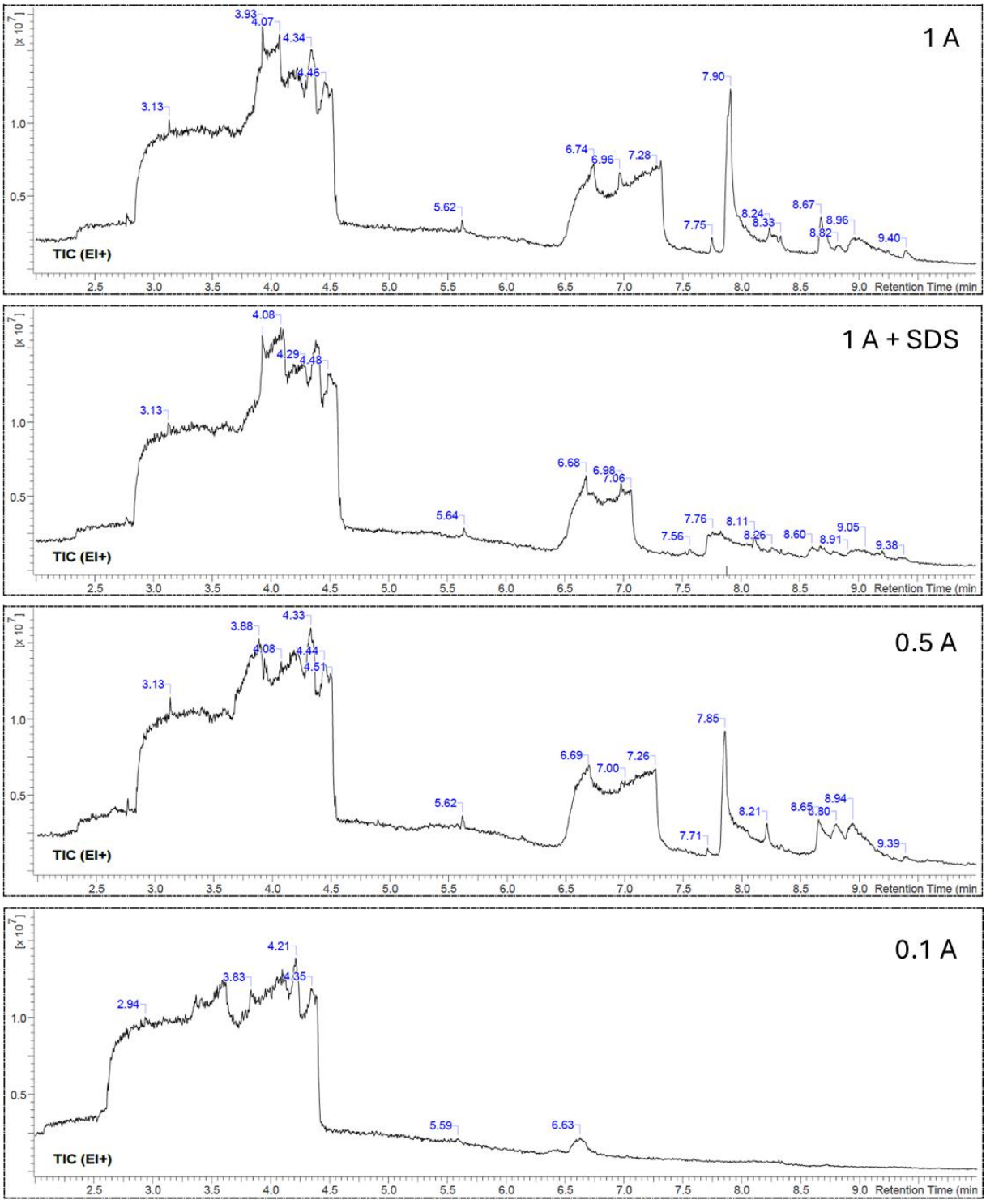

Figure S22: comparison of total ion chromatograms obtained for GC-MS analysis of samples from different desorption experiments: 1 A, 1 A + 0.52 mM SDS, 0.5 A and 0.1 A.

Table S4: peak identification for MEA oxidation products detected by GC-MS, assigned from electron-ionization (EI) mass-spectral fragmentation patterns using the NIST mass spectral library.

Retention time (min)	Compound	Structure	Remark
2.8 – 4.6	Monoethanolamine	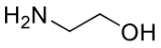	
3.1	Oxazole, 4,5-dihydro-2-methyl-	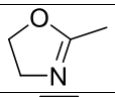	
3.9	Piperazine	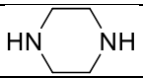	
4.1	Anisole	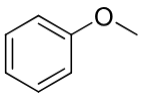	Possibly instrument contamination from previous measurements
4.3	Piperazine, ethyl-	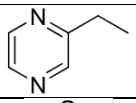	
4.4 – 8.3	Sulfur dioxide		
5.6	Unknown		No good library hits
6.7	Oxazolidin-2-one	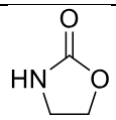	
7.0	1-Piperazine carboxaldehyde	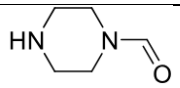	
6.4 – 7.4	Unknown		No good library hits
7.7	2-Imidazolidinone	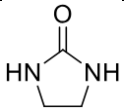	
7.8	1-(2-Hydroxyethyl) pyrazole	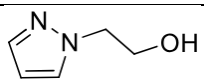	
8.2	N-(2-Hydroxyethyl) succinimide	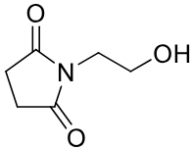	
8.3	Unknown		No good library hits
8.6	2-(2-Hydroxyethylamino) pyrimidine	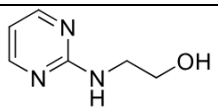	
8.8 + 8.9	Unknown		No good library hits
9.0	1-(2-Hydroxyethyl)-2-imidazolidinone	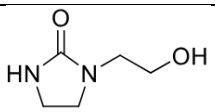	
9.4	Unknown		No good library hits

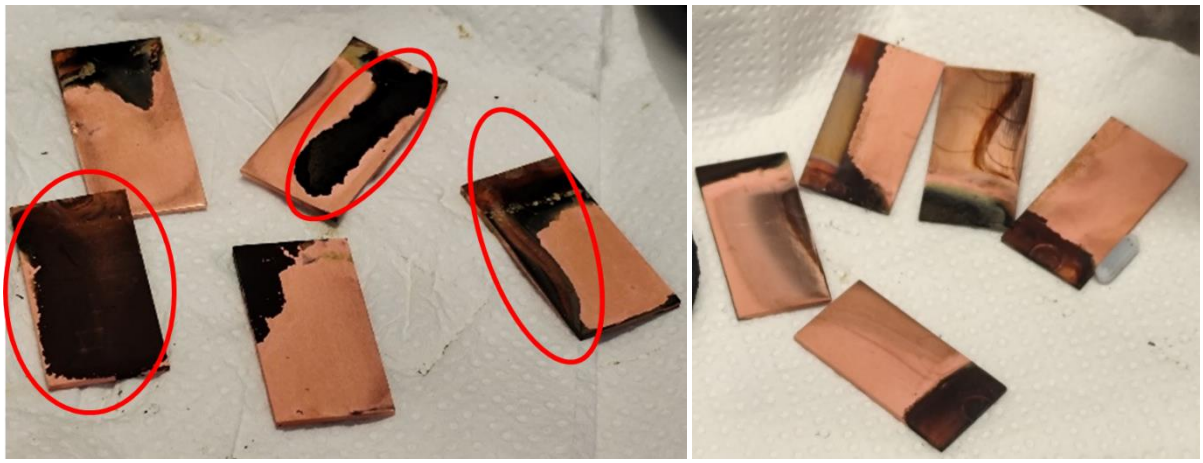

Figure S23: Cu WEs after desorption experiments at 1 A for 5 M MEA + 0.3 M Na_2SO_4 CO_2 saturated solutions, without (left) or with (right) SDS. Large dark oxide regions are indicated by red circles on the WEs used in the experiment without SDS (left picture).

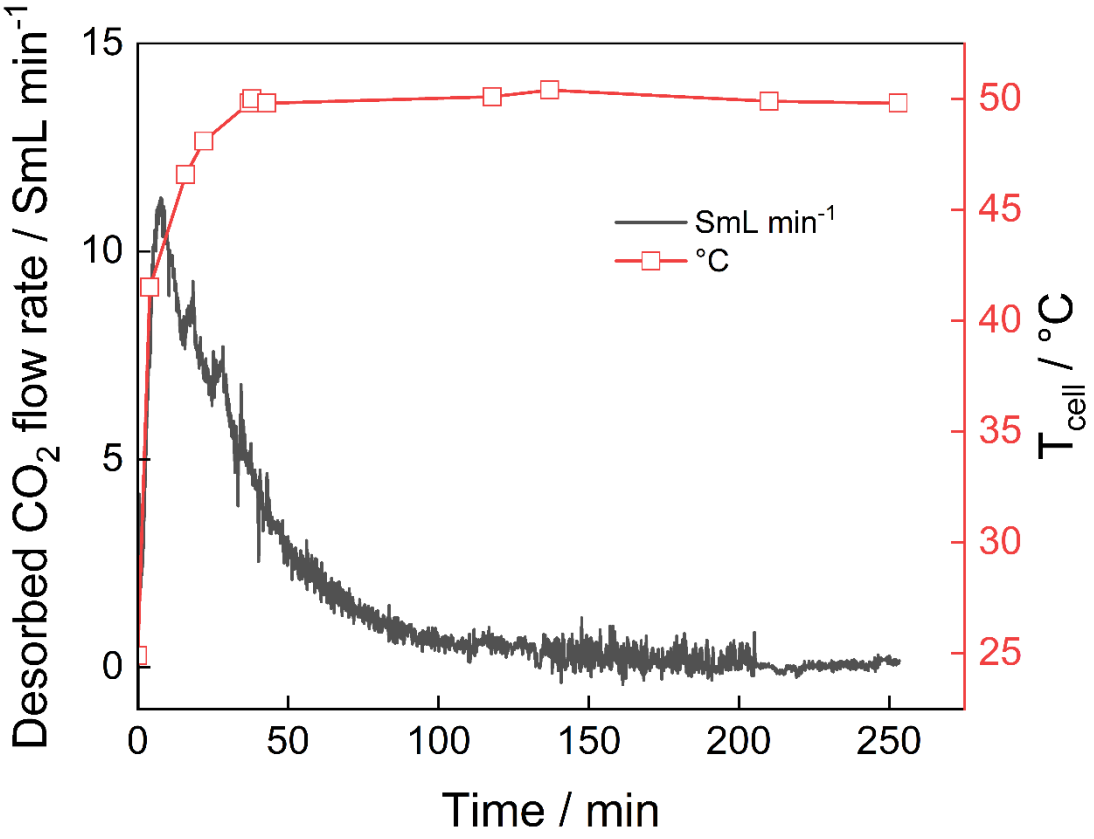

Figure S24: Temperature-driven CO_2 desorption control experiment (no current applied). CO_2 desorption profile of 5 M MEA + 0.3 M Na_2SO_4 (60 mL) pre-equilibrated and CO_2-saturated at 25 °C, then heated from 25 to 50 °C, 500 rpm stirring.

Figure S24 shows a blank desorption test performed without current or Cu electrodissolution: the MEA solution was first CO_2-saturated at 25 °C and then heated (by using a heating jacket) under temperature control to 50 °C (500 rpm stirring). Upon heating, CO_2 is released as the equilibrium CO_2 loading decreases with temperature; the outlet flow peaks during the first minutes of test and decays progressively approaching zero as the new saturation state at 50 °C is reached. The total CO_2 released (time integral of the outlet CO_2 flow rate) corresponds to ~428 SmL (0.0175 mol_{CO_2}) from 60 mL of CO_2-saturated MEA solution at 25 °C (0.058 mol_{CO_2} mol^{-1}_{MEA}), in agreement with the expected decrease in CO_2 solubility between 25 and 50 °C—*i.e.*, 3.18 to 2.86 mol_{CO_2} L^{-1}, or 0.635 to 0.572 mol_{CO_2} mol^{-1}_{MEA}, respectively.

.

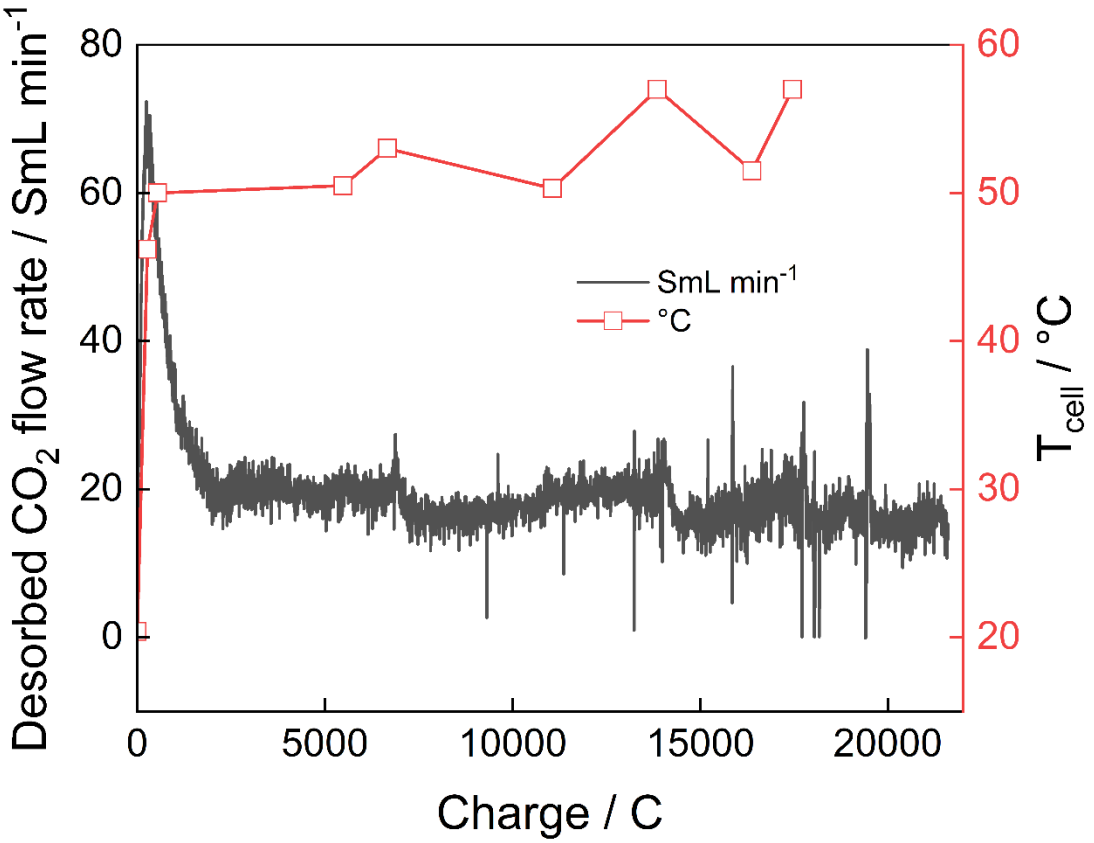

Figure S25: CO_2 desorption flow-rate profile and electrolyte temperature monitoring during a desorption experiment performed at 1.5 A without active temperature control, using 60 mL of MEA solution pre-equilibrated and CO_2-saturated at 25 °C.

Figure S25 presents a desorption experiment performed without active temperature control using a solution pre-equilibrated and CO_2-saturated at 25 °C. In the absence of temperature control, the cell temperature rises rapidly at the start, driven primarily by ohmic (Joule) heating in the relatively resistive MEA electrolyte. This transient heating produces an initial surge in the CO_2 outlet flow, consistent with thermally driven CO_2 desorption (reduced CO_2 solubility and temperature-shifted equilibria) in addition to Cu electrodissolution-driven release. Once the cell reaches ~50–60 °C and the temperature stabilizes, the CO_2 flow correspondingly levels off.

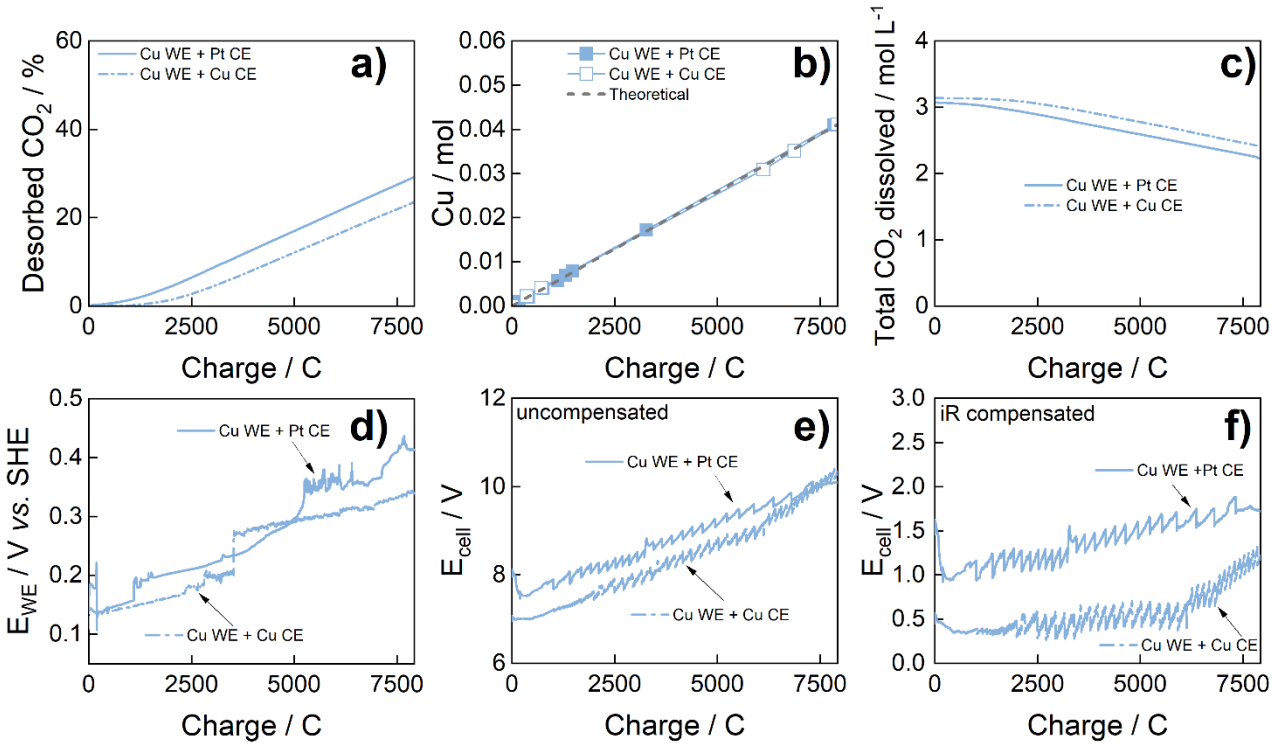

Figure S26: CO_2 desorption from CO_2-saturated 5 M MEA + 0.3 M Na_2SO_4 at 25 °C and 0.1 A, comparing the half-EMAR configuration (Cu WE + Pt CE; solid light-blue line) and the full-EMAR (co-electrodeposition) configuration (Cu WE + Cu CE; light-blue dash-dot line). Shown as a function of passed charge: (a) cumulative CO_2 desorbed (%), (b) dissolved Cu (mol) together with the theoretical Cu expected from Faraday's law (dashed grey line), (c) total dissolved inorganic carbon concentration (mol L^{-1}), (d) WE potential (V vs. SHE), (e) uncompensated cell voltage, and (f) iR-compensated cell voltage. Experiments were performed at controlled temperature (25 °C) with Ag/AgCl RE and stirring at 500 rpm. Electrodes: Cu WE (five plates; total geometric area 49.5 cm^2); for the full-EMAR case, Cu CE (two plates; 19.2 cm^2 each; total geometric area 38.4 cm^2) for Cu electrodeposition. The desorption compartment contained 60 mL of CO_2-saturated electrolyte (5 M MEA + 0.3 M Na_2SO_4). For the half-EMAR experiment, the counter compartment contained 60 mL of the same CO_2-saturated electrolyte (Cu-free). For the full-EMAR experiment, the counter compartment contained 60 mL of filtered CO_2-saturated electrolyte previously used in a desorption experiment (0.61 mol L^{-1}).

Figure S27: Copper counter electrode after experiment of full EMAR system. Catholyte: 60 mL filtered 5 M MEA + 0.3 M Na_2SO_4 CO_2 saturated after desorption experiment (with Cu ions in solution); current applied: 0.1 A; stirring: 500 rpm. The growth region is indicated with a light blue circle.

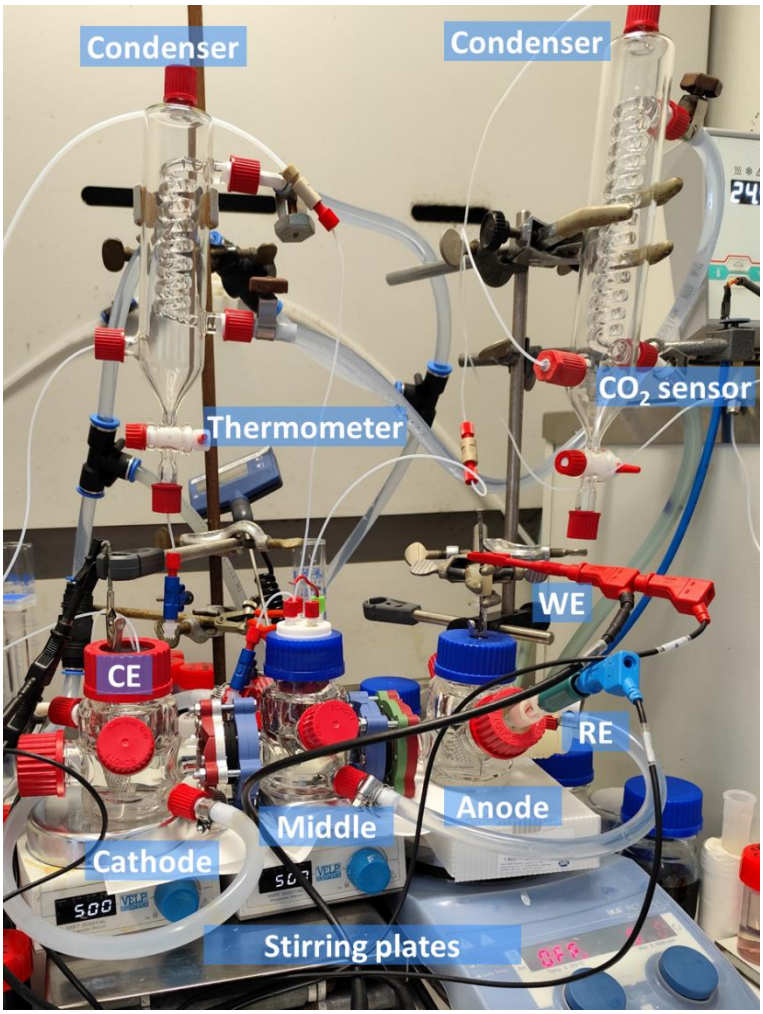

Figure S28: three-compartment cell setup used for the study of the pure e-acidification on the CO_2 desorption. indicated are: cathode and anode side, WE, RE, CE, thermometer, condensers, CO_2 sensor. Not depicted: MFM and cooling bath.

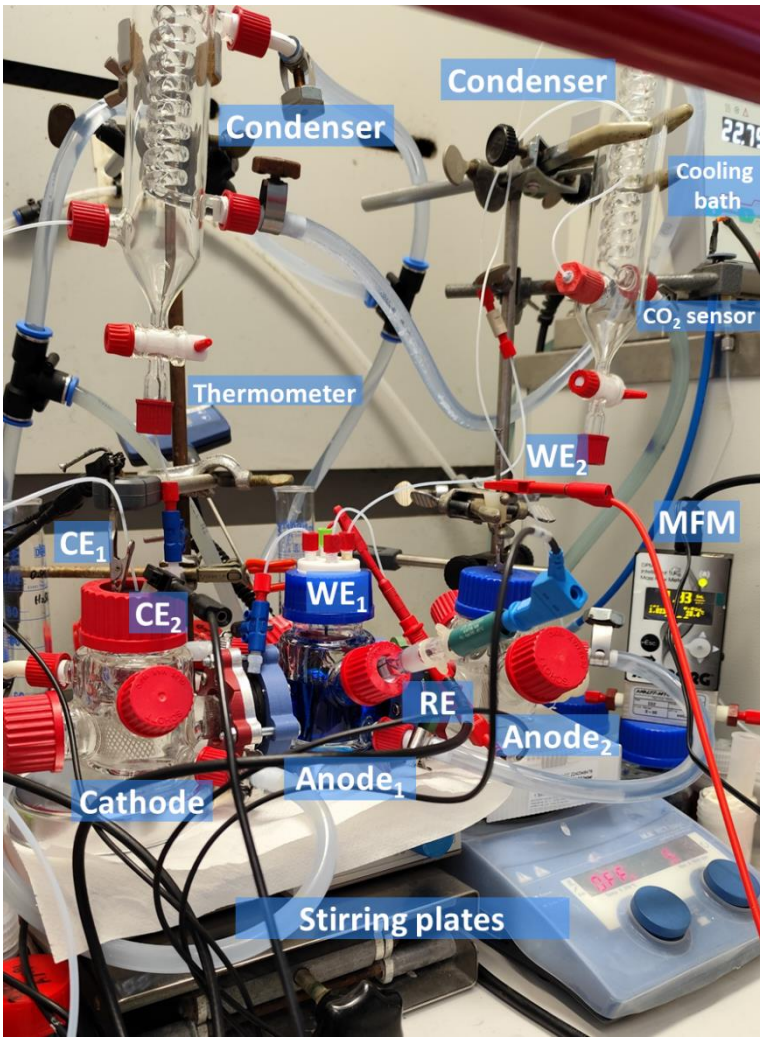

Figure S29: three-compartment cell setup used for the study of the combined e-dissolution and e-acidification on the CO_2 desorption. indicated are: cathode and anode side, WE_1, WE_2, RE, CE_1, CE_2, thermometer, condensers, MFM, CO_2 sensor, cooling bath.

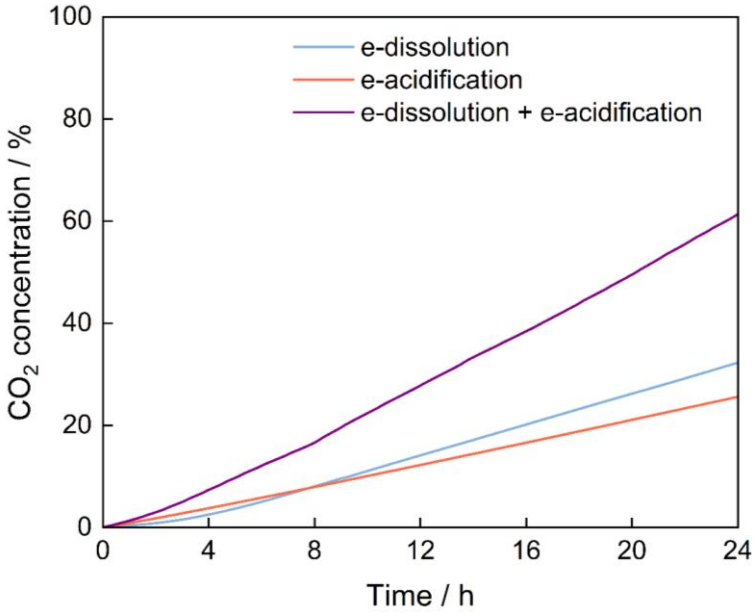

Figure S30: percentage of CO_2 desorbed from the 5 M MEA + 0.3 M Na_2SO_4 CO_2 saturated solution vs time, at 0.1 A, for e-dissolution (light blue), e-acidification (light red) and e-dissolution + e-acidification (purple).

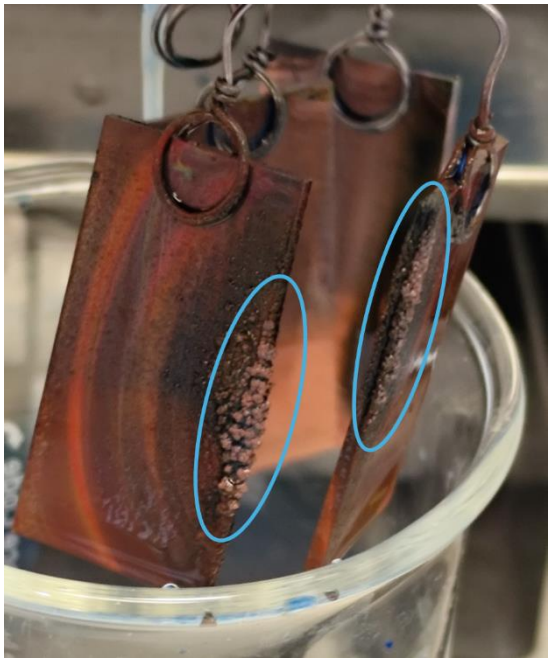

Figure S31: picture of the Cu WE after the combined e-dissolution + e-acidification. Growth regions are indicated with light blue circles.

Table S5: mass of Cu electrodes before and after the e-dissolution + e-acidification experiment. Calculated mass variation (Δm) per electrode and the corresponding electrochemical processes (electrodeposition – ED – or dissolution) are indicated.

Cu mass / g					
Before		**After**		**Δm**	**Process**
1	3.8759	**1**	4.0833	0.1631	ED
2	3.9923	**2**	2.8800	-1.0402	dissolution
3	3.8955	**3**	2.6442	-1.2760	dissolution
4	3.9456	**4**	3.2839	-0.6363	dissolution
5	3.8916	**5**	4.2668	0.3466	ED

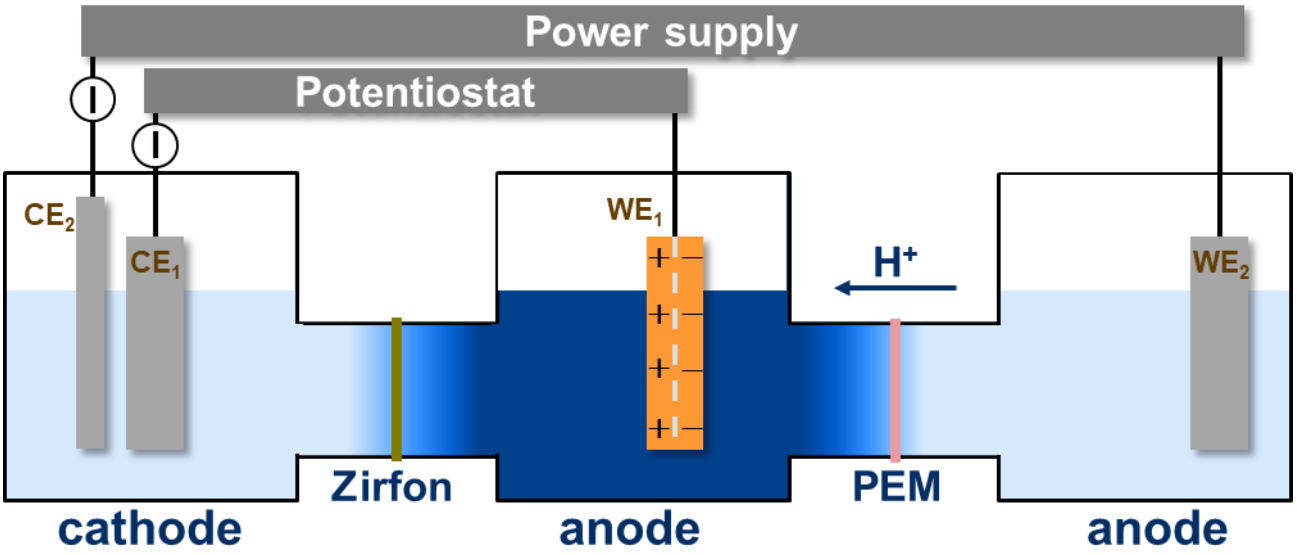

Figure S32: simplified scheme of the three-compartment cell showing the polarization of the WE_1 by influence of WE_2 (anode) and CE_2 (cathode).

Table S6: Effect of applied current on CO_2 desorption performance (Q = 10,800 C, T =25 °C).

Current / A	CO_2 desorbed / %	Cu dissolved / mol	Average CO_2 flow / SmL min^{-1}	Faradaic efficiency / %
1	51.0	0.0225	12.08	40.3
0.5	45.5	0.0293	4.94	52.4
0.1	41.7	0.0543	0.84	97.1

Table S7: Influence of SDS and temperature on CO_2 desorption at 1 A (Q = 12,000 C).

Experiment	CO_2 desorbed / %	Cu dissolved / mol	Average CO_2 flow / SmL min^{-1}	Faradaic efficiency / %
1 A, 25 °C	57.87	0.02518	12.08	40.5
1 A, 25 °C, 0.52 mM SDS	56.55	0.03979	12.35	64.0
1 A, 50 °C	56.25	0.04730	10.33	76.0

Table S8: Comparison of half EMAR (Cu WE + Pt CE) and full EMAR (Cu WE + Cu CE; anodic Cu electrodissolution and CO_2 release coupled with cathodic Cu electrodeposition and recovery configurations at 0.1 A (Q = 7,920 C, T =25 °C).

Experiment	CO_2 desorbed / %	Cu dissolved / mol	Average CO_2 flow / SmL min^{-1}	Faradaic efficiency / %
Cu WE + Pt CE	29.20	0.04146	0.8392	101
Cu WE + Cu CE	23.52	0.04113	0.7071	100

Table S9: CO_2 desorption metrics for Cu-electrodissolution, electro-acidification, and coupled operation (Q = 8,640 C, T =25 °C).

Experiment	CO_2 desorbed / %	Cu dissolved / mol	Average CO_2 flow / SmL min^{-1}	Faradaic efficiency / %
e-dissolution, 1 A	39.70	0.02008	12.08	44.8
e-dissolution, 0.1 A	32.28	0.0464	0.8392	103
e-acidification	25.60	-	0.7900	-
e-dissolution + e-acidification	27.81	0.01988	1.7826	88.8

Table S10: Anolyte pHs before and after the corresponding desorption experiments.

Experiment	pH before	pH after
1 A, 25°C	7.97	8.02
1 A, SDS, 25°C	7.77	-
1 A, 50°C	8.42	7.78
0.5 A, 25°C	7.92	7.79
0.1 A, 25°C	7.90	7.52
0.1 A, 25°C, co-ED anolyte	8.07	7.12
0.1 A, 25°C, e-acidif	7.96	7.77
0.1 A, 25°C, e-disol+e-acidif	7.87	7.11

Table S10 displays the anolyte pH before and after each experiment. Owing to the buffering capacity of the MEA/CO_2 system—including MEA/$MEAH^+$ as well as bicarbonate/carbamate equilibria—only moderate pH shifts were observed, with no drastic pH changes.

Table S11: pH evolution in the desorption compartment during the 0.1 A, 25 °C electro-acidification experiment in a three-compartment cell (WE: Pt–Ti mesh; RE: Ag/AgCl; CE: Pt–Ti mesh), reported as a function of time and passed charge.

Time / h	Charge / C	pH
0	0	7.93
1	360	7.96
4	1440	7.92
17	6120	7.85
24	8640	7.77

Table S12: pH evolution in the desorption compartment during the 0.1 A, 25 °C combined electrodissolution + electro-acidification experiment in a three-compartment cell, reported as a function of time and total passed charge (WE_1 + WE_2). The two working electrodes were operated at fixed current (0.1 A each): WE_1 = Cu (5 Cu plates, total area 49.5 cm^2) for copper electrodissolution, and WE_2 = Pt–Ti mesh for electro-acidification. Counter electrodes: CE_1 = Pt–Ti mesh and CE_2 = Pt wire; RE = Ag/AgCl. Stirring: 500 rpm in each compartment. Separators: Zirfon 500 between cathode and desorption compartments, and Nafion 117 (PEM) between desorption and acidification compartments. Electrolytes are indicated in Figure 6.

Time / h	**Charge (WE_1+WE_2) / C**	**pH**
0	0	7.87
1	720	7.83
2	1440	7.70
18	12960	6.95
24	17280	7.11